CLAS−Note 2011−018

CLAS12 FTOF Studies: Rate and Magnetic Shielding Effects on PMT Timing Resolutions

D.S. Carman and V. Baturin

October 21, 2011

Abstract

This note details the results of two different measurement test plans for the CLAS12 FTOF detector. The first study investigated the timing performance of the panel-1b R9779 PMTs as a function of rate. The second study investigated the design of the nominal magnetic shielding for the panel-1a and panel-2 PMTs by studying the timing resolution as a function of the external field. The main results of these studies are that the R9779 PMT is not expected to be rate limited in the CLAS12 environment in terms of its timing performance and that the existing magnetic shields for the panel-1a and panel-2 PMTs are expected to be adequate in the fringe fields of the CLAS12 magnets.

1 Introduction

1.1 FTOF System Overview

The Forward Time-of-Flight (FTOF) system will be a major component of the CLAS12 detector used to measure the time-of-flight of forward-going charged particles emerging from the target. The average path length from the target to the FTOF counters will be roughly 650 cm. The requirements for the FTOF system include excellent timing resolution for particle identification and good segmentation for flexible triggering and prescaling options. The design parameters were chosen to allow for separation of pions and kaons up to roughly 3 GeV. The most energetic particles are produced at small angles. The system specifications call for a time resolution of σ_{TOF}=80 ps at the more forward angles of CLAS12 and 150 ps at angles larger than 36°. The system must also be capable of operating in a high-rate environment. The maximum counting rate occurs in the forward direction where, at an operating luminosity of 1×10^{35} cm^{-2}s^{-1}, the average rate per scintillator is approximately 250 kHz. Also the PMTs will be positioned in the fringe field of the CLAS12 superconducting torus and solenoid magnets and must be shielded to minimize effects on their performance.

The FTOF system will also be used for energy-loss measurements in specific instances. Pulse height information, being directly proportional to energy deposited, provides an independent means for the identification of slow particles. In this regard, the flight time can provide for a more accurate measurement of particle energy than magnetic analysis for slow particles, where the effects of multiple scattering are the largest.

In order to meet the requirements for the tight timing resolution, the major considerations in the design of the FTOF system are:

- *Scintillator Size:* The overall size of the system will demand careful consideration of light collection in order to optimize the time resolution of the system. Also, the width of each scintillator determines the granularity of the scattering angle definition in the trigger.

- *Geometry:* The projected space behind the coils of the main CLAS12 torus is inactive and therefore useful for locating the light guides, photomultiplier tubes (PMTs), voltage dividers, and cables. The remaining area in the forward direction is the fiducial region of the detector and must be covered with scintillator counters.

- *Magnetic Field:* The PMTs will have to be properly shielded from the stray magnetic fields of the CLAS12 torus and solenoid.

- *Crossing Tracks:* Particle trajectories from the target can intersect adjacent TOF counters. Therefore light from both counters will have to be summed to optimize particle identification in the data analysis.

In each sector of CLAS12, the FTOF system will be comprised of three sets of TOF counters, referred to as panels (called panel-1a, 1b, and 2). Each panel consists of an array of rectangular scintillators with a PMT on each end. Panel-1 refers to the sets of counters located at forward angles (roughly 5° to 36°) (where the two panels are necessary to meet

the 80 ps resolution requirements) and panel-2 refers to the sets of counters located at larger angles (roughly 36° to 45°). The positioning and attachment of the FTOF system panels to the forward carriage of CLAS12 are shown in Fig. 1.

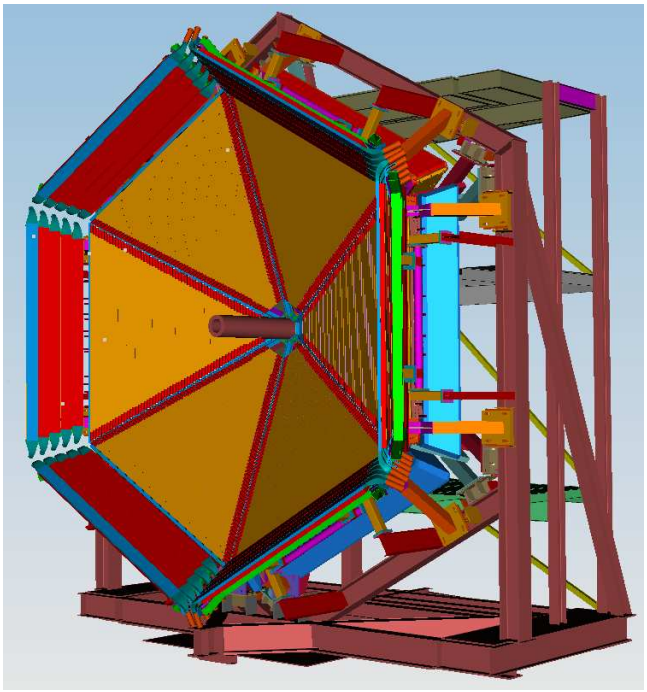

Figure 1: View of the FTOF counters for CLAS12 highlighting the location of the panel-1 and panel-2 counters.

The panel-1 counters will consist of the current CLAS panel-1 TOF counters (called panel-1a) and a new set of panel-1 counters (called panel-1b). The existing panel-1a counters consist of 23 scintillators, each measuring 5.08-cm thick and 15-cm wide. The lengths of these counters range from roughly 32 cm at the smallest scattering angles to roughly 375 cm at the largest scattering angles. The scintillators are constructed from Bicron BC-408 and are read out through short acrylic light guides to 2-in Thorn EMI-9954A PMTs (see Fig. 2). The new panel-1b counters will consist of an array of 62 scintillators constructed from Bicron BC-404 scintillator for the shorter counters and BC-408 for the longer counters, each 6-cm wide and 6-cm thick with a range from 17 to 408 cm. They are readout at each end by Hamamatsu R9779 PMTs coupled directly to the scintillators. This new panel will be mounted off of the Forward Carriage in front of the existing panel-1a counters.

The panel-2 counters will consist of 5 scintillators extracted from the current CLAS panel-2 TOF counters. These bars are 22-cm wide and 5.08-cm thick, with lengths from roughly 370 cm to 430 cm. The scintillators are constructed from Bicron BC-408 and are read out through curved acrylic light guides to 3-in Philips XP4312B PMTs (see Fig. 2). These scintillators are included to give complete acceptance for outbending charged particles incident upon the CLAS12 drift chambers. In the current CLAS detector, the panel-2 counters are mounted to the side carriages (called the North and South Clam Shells). However, in the CLAS12 design these panels will be mounted on the Forward Carriage.

Figure 2: Photograph of the 2-in EMI 9954A and 3-in Photonis XP4312B PMTs and their associated voltage dividers that are current part of the CLAS TOF system and will be used for the CLAS12 panel-1a and panel-2 FTOF arrays, respectively.

1.2 Test Plan Overview

In this note two different test plans for the FTOF PMTs were carried out. The first involved studying the time resolution of the panel-1b PMT, the Hamamatsu R9779 as a function of rate. This test plan is described in detail in Section 2. The second test plan was designed to study the performance of the existing magnetic shields for the panel-1a and panel-2 PMTs to understand if they will be adequate for the fringe field levels expected at the PMT locations arising from both the CLAS12 solenoid and the torus magnets. Note that the associated magnetic field studies for the panel-1b PMTs have already been completed and the (nearly) final design of this magnetic shield is shown in Fig. 3. This shielding is designed to provide a 2-mm-thick mu-metal box for these PMTs (in conjunction with their neighboring PMT shields).

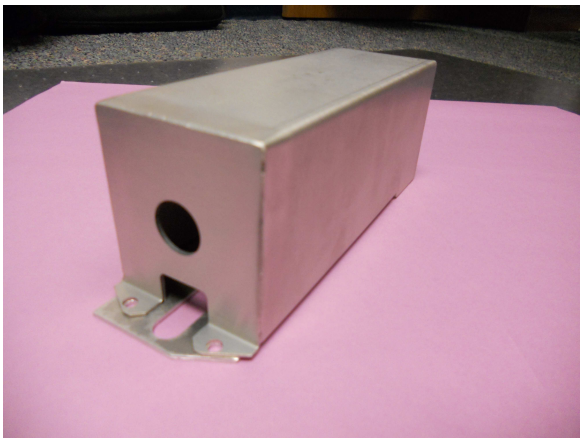

Figure 3: Photograph of the prototype magnetic shield for the panel-1b PMTs.

2 PMT Rate Studies

PMTs are designed to exhibit good linearity in anode output current over a wide range of incident light levels. However, if the intensity of incident light is too large, the output begins to deviate from the ideal linearity. This type of saturation effect implies that the output signal is no longer proportional to the incident light intensity. This effect is illustrated for a generic PMT in Fig. 4.

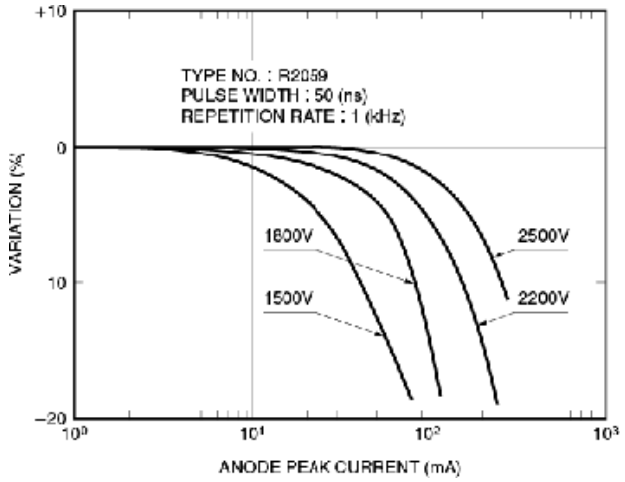

Figure 4: Voltage dependence of the linearity of a generic PMT [1].

The anode linearity is limited by two factors. One is the design of the voltage divider circuit and the second is caused by space charge effects due to a large current flowing in the dynodes, such as is the case in high rate operations and/or environments with a large amount of light entering the PMT. This causes current saturation effects in the PMT. However, the true effect is not so directly tied to the incoming photon rate, but to the anode current. However, even though the PMT response becomes non-linear and begins to saturate at higher light intensities, it is important to study the time resolution of the PMT. Effects of non-linearities could manifest themselves in a distorted pulse shape that could directly impact the PMT timing resolution, which could limit the operating luminosities of the CLAS12 detector.

2.1 Set-up

For the rate studies, the main parameter of interest for the R9779 PMT is its timing resolution. For this study, the R9779 timing resolution was studied at each point in relation to the timing resolution of a reference photodetector, the Hamamatsu 2-in R2083 PMT. The R2083 is the timing PMT that will be used for the CTOF detector and represents an 8-stage linear-focussed PMT. The test plan then amounted to measuring the ratio of the PMT timing resolutions as a function of the rate of the light source, which was varied from 5 kHz to 3 MHz.

The configuration of the PMTs in the test stand is as shown in Fig. 5. Here the light source consists of four blue LEDs (λ=475 nm) mounted equidistantly about a plastic ring

that also served as the coupling fixture for the two PMTs. This configuration was specifically designed so that each PMT symmetrically viewed the light source (i.e. both PMTs saw the same amount of light) and that the photocathodes of each PMT were uniformly illuminated. The light-flash amplitude was adjusted so that the combined light collected by the two PMTs (as measured by the summed QDC values) was about 1250 photoelectrons (see Fig. 6). More details on the set-up are contained in the CLAS-Notes of Refs. [2, 3].

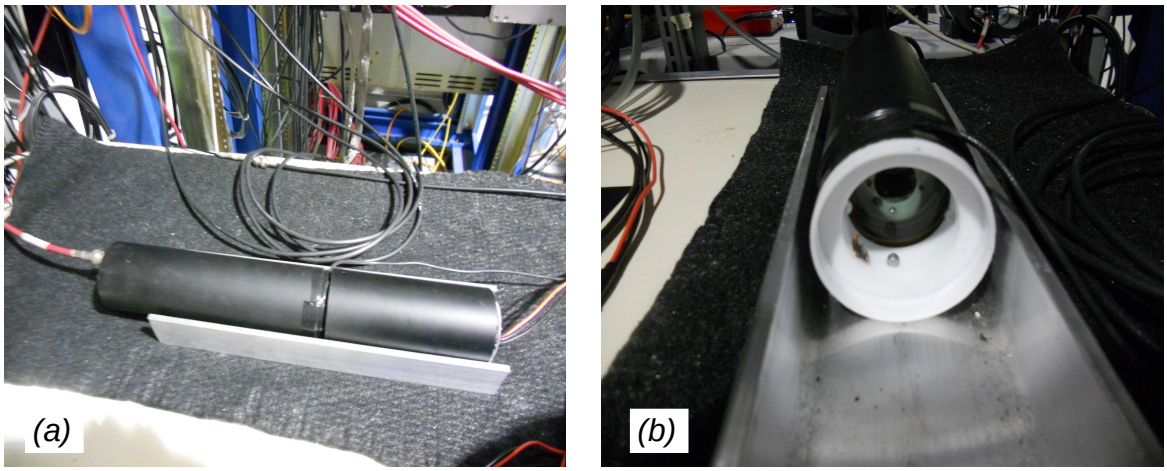

Figure 5: (a). Photograph of the coupled PMTs symmetrically viewing the pulsed blue LED light source. (b). Photograph of the light source with one PMT removed.

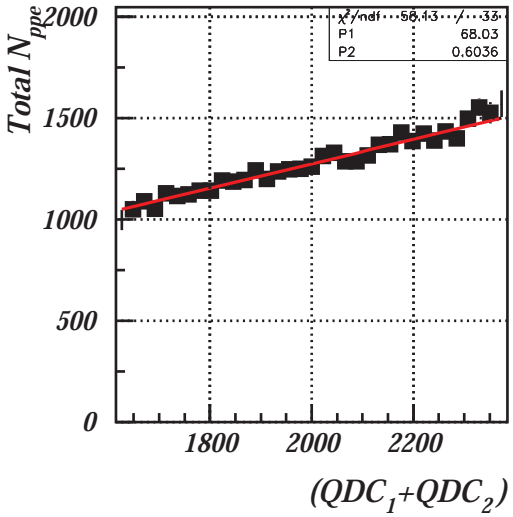

Figure 6: Measured total number of photoelectrons seen by the test and reference PMTs for the rate studies for a typical configuration.

Each PMT was connected to HV and the anode was sent to a custom 12:1 splitter. The larger output of the splitter went to a constant-fraction discriminator and then provided the TDC stop. The smaller output of the splitter went to a QDC. The pulser provided the trigger, the ADC gate, and the TDC start. The nominal voltage setting for the R2083 was V=-1500 V, which resulted in a typical measured gain $G \sim 9.0 \times 10^5$. For the R9779,

the nominal voltage setting was V=-1500 V, which resulted in a typical measured gain $G \sim 1.5 \times 10^6$. For these studies the ADC pedestals were measured immediately before the rate measurement sequence. Fig. 7 shows a photograph of the readout electronics and data acquisition system used for these tests.

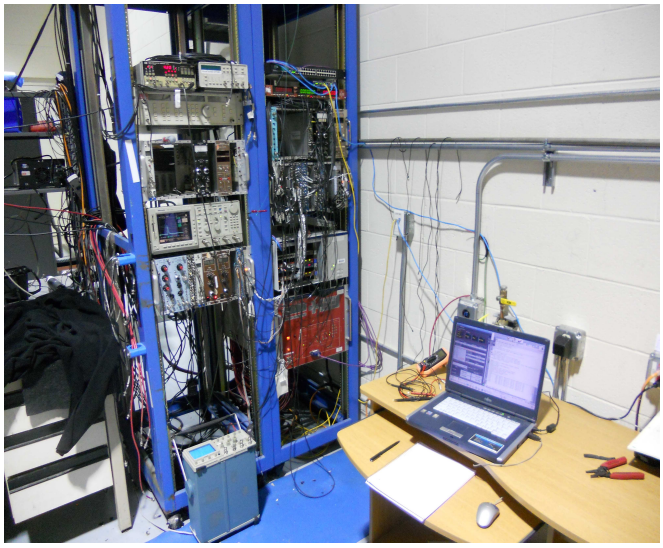

Figure 7: Photograph of the readout electronics and data acquisition system used for the FTOF PMT tests.

2.2 Results & Conclusions

The main results of these measurements are contained in Fig. 8. Here the time resolution ratio for the R9779 PMT relative to the R2083 PMT is plotted as a function of the pulser rate. The data show that the R9779 timing resolution is unchanged up to a rate of about 500 kHz. Beyond that point, both PMTs begin to enter a non-linear regime due to saturation. In an attempt to counteract this effect, the pulser amplitude was adjusted at several points to try to keep the number of primary photoelectrons seen by the reference R2083 PMT fixed (see Fig. 9). These adjustments can be seen as the steps in N_{ppe} in Fig. 9 at about 100 kHz and again at about 1 MHz. Because of the difficulties associated with the PMT saturation effects at the higher rates, i.e. values between 1 and 3 MHz, the measured time resolutions are likely only accurate to the 10% level. So, at least at this level of accuracy, the timing resolution of the R9779 PMT is maintained even to rates well beyond 1 MHz.

Fig. 9 also shows the measured number of primary photoelectrons N_{ppe} seen by each PMT as a function of pulser rate. All of the tests done here confirm the so-called "statistical law". Namely, that the PMT timing resolution is directly proportional to $1/\sqrt{N_{ppe}}$, thus the electronics component to the timing resolution is negligible.

The last aspect of this work that is required for a complete understanding of the expected PMT performance is to determine the incident flux of charged particles on the FTOF counters expected during operation at the nominal beam-target luminosity for CLAS12, namely $\mathcal{L}$=1×10^{35} cm^{-2}s^{-1}. These studies using the GEMC GEANT4 Monte Carlo simulation code [4] are now in progress. Ultimately these simulations should provide the FTOF

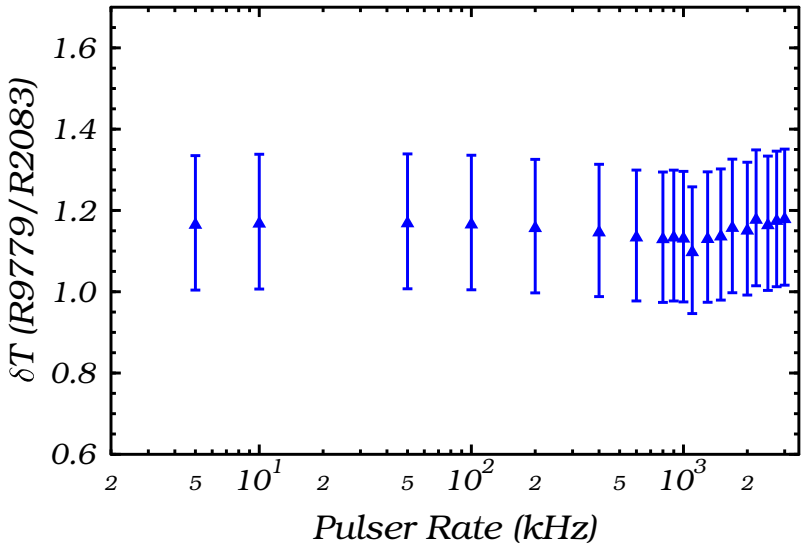

Figure 8: Main results of the PMT rate tests showing the ratio of measured PMT timing resolutions for the FTOF panel-1b R9779 PMT assembly to the CTOF R2083 PMT as a function of the light pulser rate (kHz). The error bars represent the 10% systematic uncertainty assigned to the time resolution measurements.

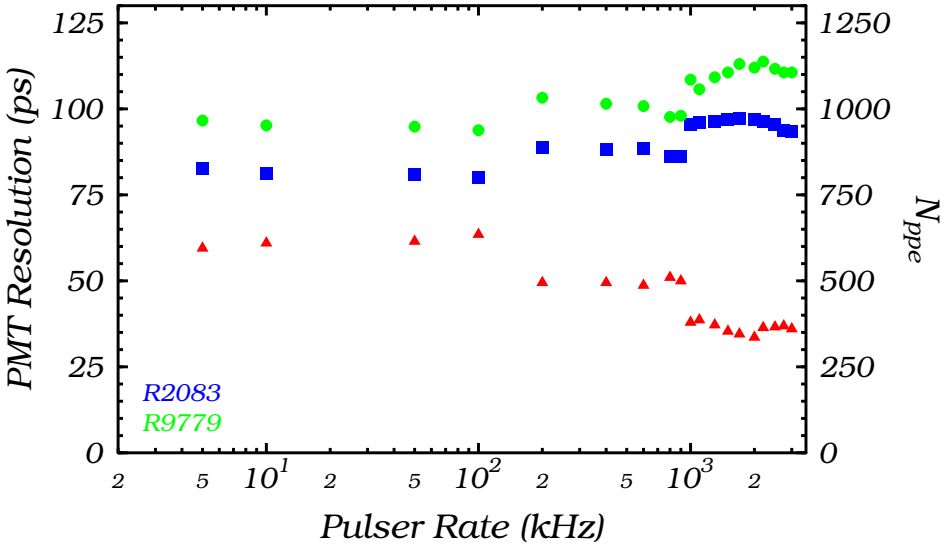

Figure 9: Measured number of primary photoelectrons (red triangles) seen by each of the PMTs (right-side scale) as a function of the pulser rate. The measured PMT timing resolutions (left-hand scale) for the R2083 PMT (blue squares) and the R9779 PMT (green circles) are also shown vs. pulser rate. Non-linear effects set in starting at around 500 kHz.

rates (fluence) expected per counter for charged particles (e,μ,π,K,p), which can be used to estimate the expected PMT anode currents.

3 PMT Magnetic Shield Studies

The scintillation bars of the panel-1a FTOF system are readout at each end by 2-in diameter Thorn EMI 9954A (Electron Tubes) PMTs. These units are a 12-stage design with a 15.9 cm^2 photocathode area. The panel-2 FTOF scintillation bars are readout at each end by 3-in diameter Photonis (Philips) XP4312B PMTs. These 12-stage PMTs have a 30.2 cm^2 photocathode area. Fig. 10 shows a schematic view of these PMTs and the magnetic shielding that is installed. This figure was taken from Ref. [5].

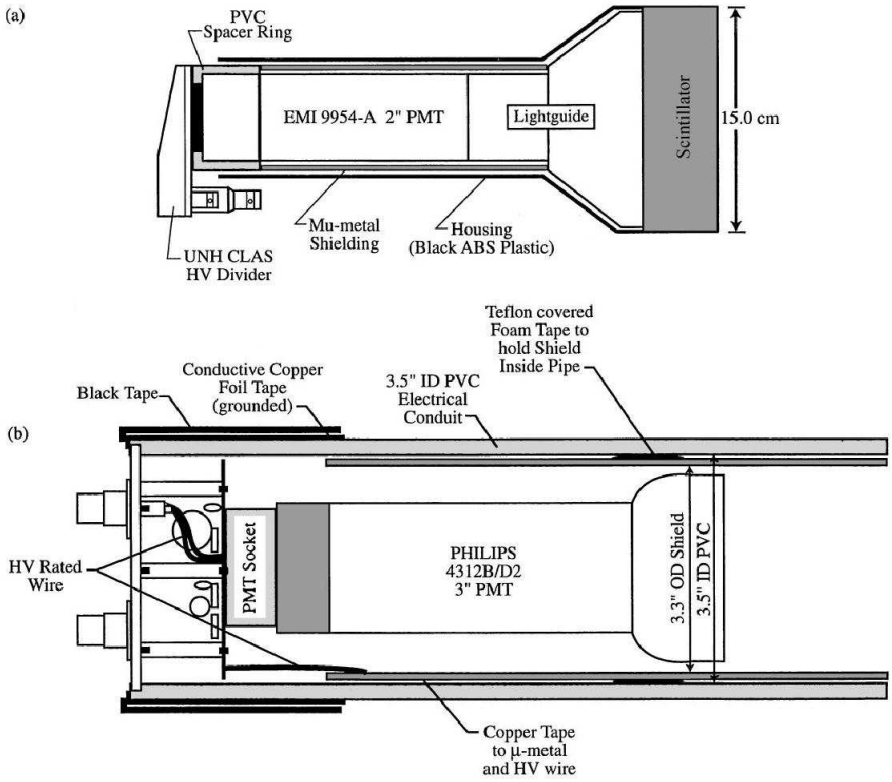

Figure 10: Side view of the PMT base assembly mounted on the CLAS TOF scintillators. (a). The readout of the CLAS panel-1 scintillation bars. This figure shows the end of the scintillator, the tapered light guide, the PMT, the voltage divider, the mu-metal shielding, and the PVC support tube. (b). The readout of the CLAS panel-2 scintillation bars. This figure shows the PMT, the voltage divider, the mu-metal shielding, and the PVC support tube. The panel-2 scintillators are connected to the PMTs through bent light guides (not shown).

The FTOF PMTs will reside in the fringe fields created mainly by the superconducting torus magnet and to a lesser extent by the superconducting solenoid magnet. The strength of the field and its direction relative to the PMT axis depends on the location of the PMT.

PMT performance is very sensitive to external magnetic fields and their output diminishes very rapidly in the presence of such fields. In order to ensure that the intrinsic timing resolution is not affected due to the loss of signal and the distortion of the pulse shape, the external fields must be well known and appropriate magnetic shielding must be designed.

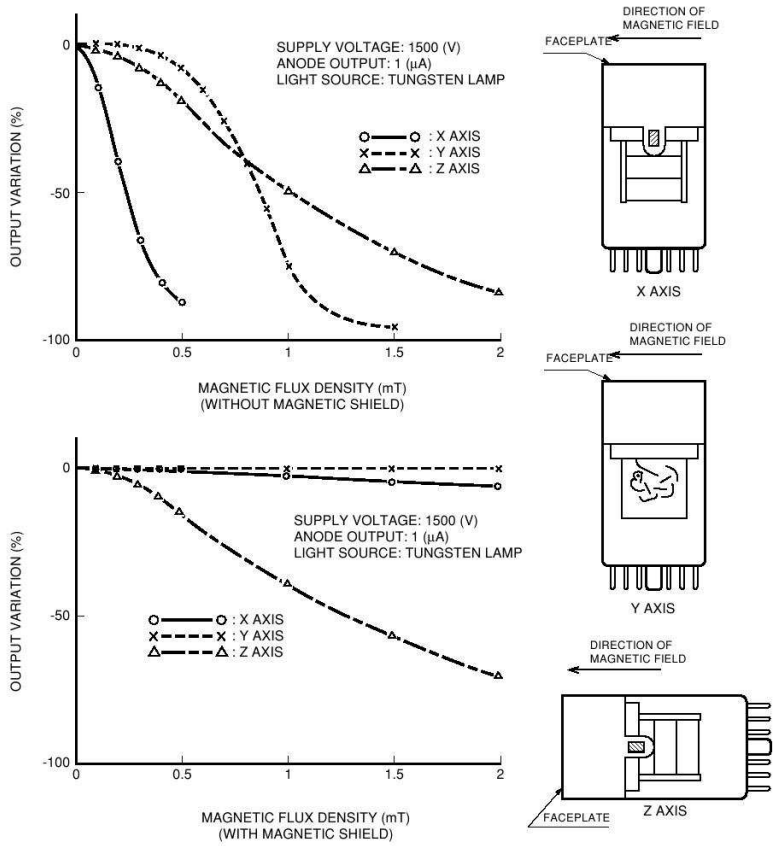

Figure 11: Performance characteristics of generic head-on PMT in axial and transverse fields [1].

Fig. 11 shows the effect of transverse and axial magnetic fields on the output of a generic head-on PMT for a design with and without a magnetic shield. Here, transverse refers to fields orthogonal to the axis of the PMT cylinder and axial refers to fields along the PMT axis. The designation "head-on" refers to a design where the scintillation light enters the PMT through a window at the end of the unit.

The basic mechanism of operation of a generic PMT (see Fig. 12) is that light enters the PMT through the faceplate (or input window) and impinges on a photocathode grid. These photons excite electrons in the photocathode so that photoelectrons are emitted, which are then accelerated due to a potential difference between the focussing electrode and the first dynode, where they are multiplied by means of secondary electron emission. This secondary emission process is repeated at each of the successive dynodes in the PMT producing a macroscopic current that can be readout. The secondary emitted electrons at the last dynode stage are finally collected at the anode.

External magnetic fields deteriorate the performance of the PMTs in two ways:

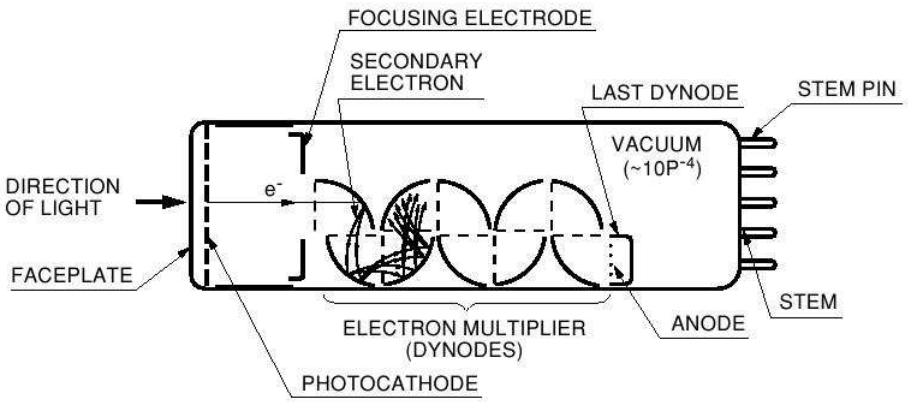

Figure 12: Construction of a generic head-on type photomultiplier tube [1].

- Decrease the efficiency of the photoelectron collection. A fraction of the photoelectrons created at the photocathode are deviated from their normal trajectories by the magnetic field due to the $\vec{v}_e \times \vec{B}$ Lorentz force and do not reach the first dynode.
- Perturbate the electron multiplication. The magnetic field also deviates the trajectories of secondary electrons going from one dynode to the next one. A fraction of them are lost, which causes a drop in the PMT gain.

Fig. 11 shows that without a magnetic shield, the signal output of a PMT is most adversely affected by transverse magnetic field components. For these components, more of the secondary electrons are swept out of the multiplication stream into the side walls of the PMT. However, there is also significant signal loss for axial magnetic field components as well due to the orientation of the dynodes in the chain and the trajectories of the secondary electrons. However, including a magnetic shield (a metal with high-permeability such as mu-metal), the PMT can be effectively shielded from the external fields and its output signal levels can be restored up until the point that the field saturates within the shield.

Fig. 11 also shows the performance of the PMT with a magnetic shield. Note that the transverse components of the field are the most easily shielded. However, because the shield design is cylindrical and open at the ends, it is not as effective in shielding the axial components of the field. A number of studies have shown that the most effective cylindrical shield for improving performance in an axial field extends past the photocathode by roughly the diameter of the PMT. In fact, the magnetic shields for the CLAS panel-1a and panel-2 PMTs follow this rule of thumb.

Full details on the design of the magnetic shields for the 2-in and 3-in PMTs is given in Ref. [5]. The magnetic shield for the panel-1a 2-in PMTs is made from a single cylinder of 0.040-in-thick mu-metal, 2.25-in in diameter and 7 in long. The shield extends 2 in beyond the front face of the PMT and was designed to shield axial fields up to about 20 G. For the 3-in PMTs, the magnetic shield is made from a single cylinder of 0.06-in-thick mu-metal, 3.32-in in diameter and 9.5 in long. The shield extends 2.5 in beyond the front face of the PMT and was designed to shield axial fields up to about 30 G. According to Ref. [5], at the location of the CLAS PMTs, the magnetic field due to the CLAS torus is roughly 2/3 axial. A photograph of the shields procured for this study is shown in Fig. 13.

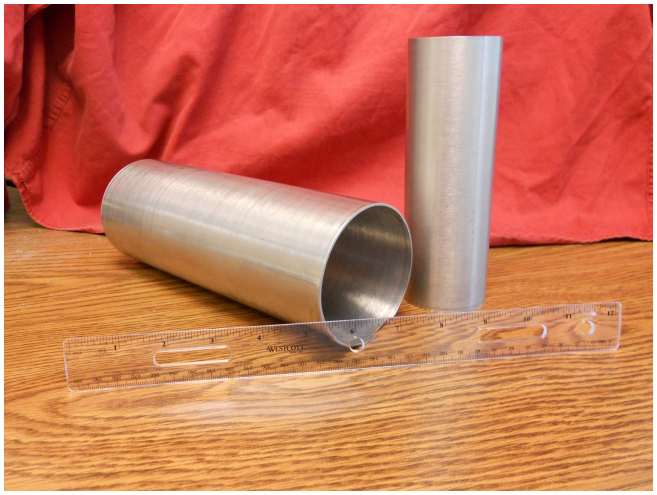

Figure 13: Photograph of the mu-metal magnetic shields used for the 2-in and 3-in PMTs presently in use for CLAS that will be used to shield the CLAS12 panel-1a and panel-2 PMTs, respectively.

For the CLAS12 FTOF magnetic shielding, the critical needed input is the strength of the magnetic field at the locations of the PMTs from the combined field from the CLAS12 solenoid and torus magnets. Using the final design positions of the FTOF PMTs for the panel-1a, panel-1b, and panel-2 PMTs (actually the (x, y, z) coordinates at the center of the end of the scintillators for one sector), the field was computed based on the "Final Design Review" magnet designs. These external magnetic field values are listed in Tables 2 to 5 in the Appendix.

The computed CLAS12 magnetic field tables show that the maximum magnetic field values are about 17 G for panel-1a, 22 G for panel-1b, and 28 G for panel-2. Given the maximum expected field for which the panel-1a and panel-2 shield were designed for in CLAS, namely about 20 G and 30 G, respectively, it seems that the shielding factors might be expected to be adequate. Again, as was the case for the CLAS torus design, for CLAS12, roughly 2/3 of the field will be along the PMT axis (axial).

3.1 Set-up

For the magnetic field studies, the main PMT parameter of interest for the test PMTs, namely the 2-in 9954A and 3-in XP4312B, is the PMT timing resolution. For all studies, the PMT timing resolutions were studied in relation to the timing resolution for a reference PMT, the field immune 39-in diameter R5924 fine-mesh PMT from Hamamatsu. The test plan then amounted to measuring the ratio of PMT timing resolutions between the test and reference PMTs as a function of external field in the range from 0 to 60 G.

A magnetic field was created at the location of the PMTs by a set of Helmholtz coils with a diameter of ≈66 in. The field intensity of this configuration was designed to reach a maximum of ≈100 G. The field strength at the location of the PMTs was measured with a Hall probe with an accuracy of about 0.2 G. The test plan studied the time resolution ratios as a function of field strength for three different magnetic field configurations. In the first

study, the PMT cylinder axis was parallel to the field direction (the axial configuration). In the second, the PMT cylinder axis was at 45° with respect to the field direction. In the third configuration, the PMT cylinder axis was positioned transverse to the field direction. Fig. 14 shows several photographs of the Helmholtz coils. The coils were powered with a Sorensen DCR 55-180T power DC power supply (0-55 V, 0-180 A). Fig. 15 shows the box between the coils where the PMTs were set up. For all magnetic field orientations, the configuration within the test box remained fixed. The PMTs were oriented with respect to the field by rotating the box within the coils using an external vernier with an accuracy of ±5°.

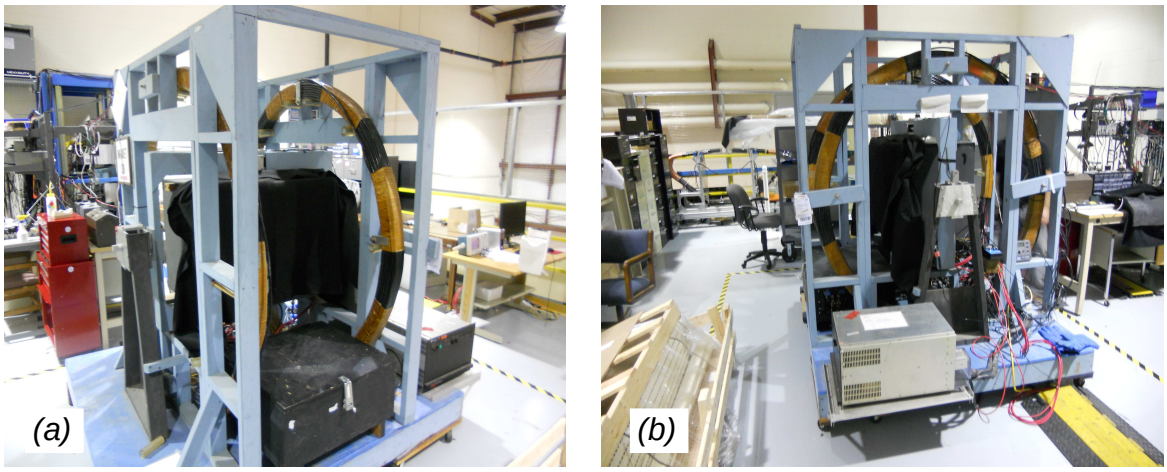

Figure 14: Photographs of the Helmholtz coils and support frame used for the PMT magnetic shield tests. The PMTs under study were placed in the rotatable box between the coils.

Figure 15: Photograph inside the rotatable box showing one configuration of the PMT test setup. Either the 2-in panel-1a PMT or the 3-in panel-2 PMT was coupled to the field-resistant R5924 fine-mesh PMT. Both PMTs viewed the same light source.

The PMTs were set-up inside the shield housing viewing a pink LED system (λ=475 nm) whose frequency was controlled by an external pulser set to a rate of 10 kHz. The light-flash amplitude was adjusted so that the combined light collected by the two PMTs (as measured

by the summed QDC values) was about 2000 photoelectrons for the 3-in PMT tests and about 1250 photoelectrons for the 2-in PMT tests (see Fig. 16). The 4 LEDs were mounted equidistantly around the perimeter of a plastic ring, similar in design to that shown in Fig. 5. This configuration was designed to uniformly illuminate the PMT photocathodes.

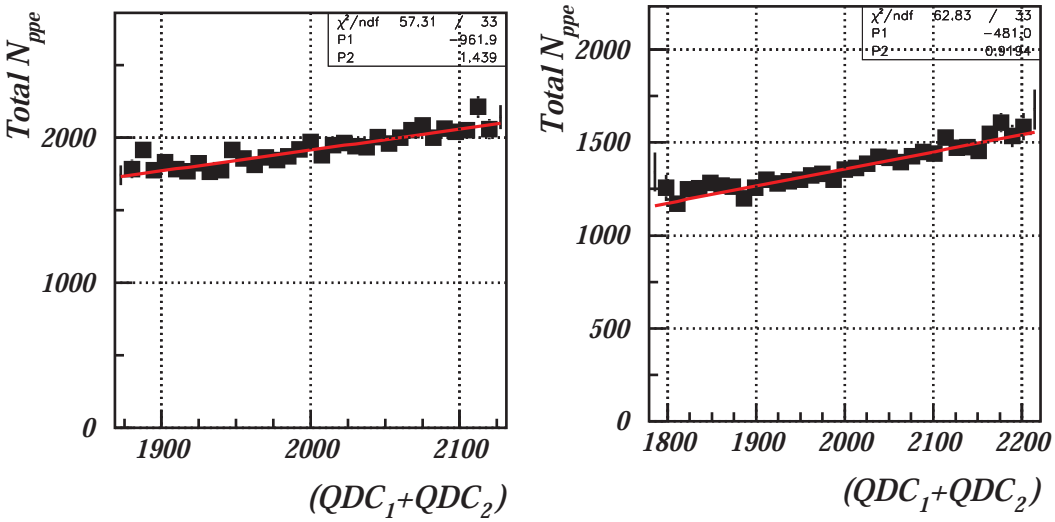

Figure 16: Measured total number of photoelectrons seen by the test and reference PMTs for (left) the 3-in PMT studies and (right) the 2-in PMT studies.

Each PMT was connected to HV and the anode was sent to a custom 12:1 splitter. The larger output of the splitter went to a constant-fraction discriminator and then provided the TDC stop. The smaller output of the splitter went to a QDC. The pulser provide the trigger, the ADC gate, and the TDC start. The nominal voltage setting for the R5924 was V=-1500 V, which resulted in a typical measured gain G= 2.0×10^6. For the 3-in XP4312B, the nominal voltage setting was V=-1700 V, which resulted in a typical measured gain $G \sim 5 \times 10^6$. For the 2-in 9954A, the nominal voltage setting was V=-1975 V, which resulted in a typical measured gain of $G \sim 5 \times 10^6$. For these studies, the ADC pedestal was measured at 0 pulser amplitude with and without the Helmholtz power supply energized at 0 V and found to be the same. For each measurement PMT and field configuration, the timing resolution ratio was measured at zero field and then after the measurement program was completed, another zero field measurement was completed.

Due to the fact that the R5924 PMT and light source was inserted into the end of the magnetic shield for both shield and PMT configurations, the amount of light seen by the reference and test PMTs was not the same. Thus the specific value of the time resolution ratio is not entirely meaningful. In fact, we have tracked the performance of the 2-in 9954A and 3-in XP4312B PMT through the ratio of their time resolutions with respect to the field immune PMT, whose response was relatively constant over all configurations of field and orientation.

3.2 Results & Conclusions

The main results of these studies are shown in Fig. 17. On the left-hand side of this figure are the studies with the 3-in XP4321B PMT and on the right-hand side of this figure are

the studies with the 2-in 9954A PMT. The time resolution ratio of the test PMTs relative to the reference PMT was studied as a function of the magnetic field over the range from 0 to 60 G. For each PMT, the time resolution ratio was studied for an axial, 45°, and transverse field configuration.

The data show that with the magnetic shield employed, there is no measurable impact on the test PMT timing resolution for a purely transverse field. For the other field configurations (axial and 45° orientations), the timing resolution slowly degrades as the external field value increases. Simple linear fits have been employed to quantify this degradation as shown in Table 1.

3-in XP4312B PMT	
Axial field 0 to 35 G	-0.2%/G
45° field 0 to 45 G	-0.1%/G
2-in 9954A PMT	
Axial field 0 to 40 G	-0.1%/G
45° field 0 to 45 G	-0.05%/G

Table 1: Approximate timing resolution loss as a function of external magnetic fields using the nominal shielding for the 2-in 9954A and 3-in XP4312B PMTs.

Given that the resolution remains within 10% of the zero field value for the 3-in XP4312B PMT up to 35 G (25% larger than the maximum computed field magnitude) and within 5% for the 2-in 9954A PMT up to 40 G (100% larger than the maximum computed field magnitude) (of which, like CLAS, roughly 2/3 of the field is axial), the conclusion is that the existing magnetic shields for the panel-1a and panel-2 PMTs are considered adequate to meet the FTOF counter timing resolution specifications for these counters. Note that beyond these field levels, the degradation in timing resolution becomes non-linear and quickly falls off. The onset of this effect occurs when the shield is fully saturated and cannot contain the external field. Field levels at the location of the PMT (i.e. within the shield), quickly rise above 0.5 to 1 G and the PMT functionality is compromised.

References

[1] Photomultiplier Tubes Basics and Applications, Third Edition, Hamamatsu Corp. 2006.

[2] V. Baturin *et al.*, *"TOF Resolution Measurements with the CLAS12 Central TOF Detector with Fine-Mesh Photomultiplier Tubes"*, CLAS-Note 2011-005, (2009).

[3] V. Baturin *et al.*, *"Time Resolution Measurements with the Final Prototype for the CLAS12 Central TOF Detector"*, CLAS-Note 2009-001, (2011).

[4] GEMC, GEANT4 simulation of the CLAS12 detector. See http://gemc.jlab.org.

[5] E.S. Smith *et al.*, Nucl. Instr. and. Meth. A **432**, 265 (1999).

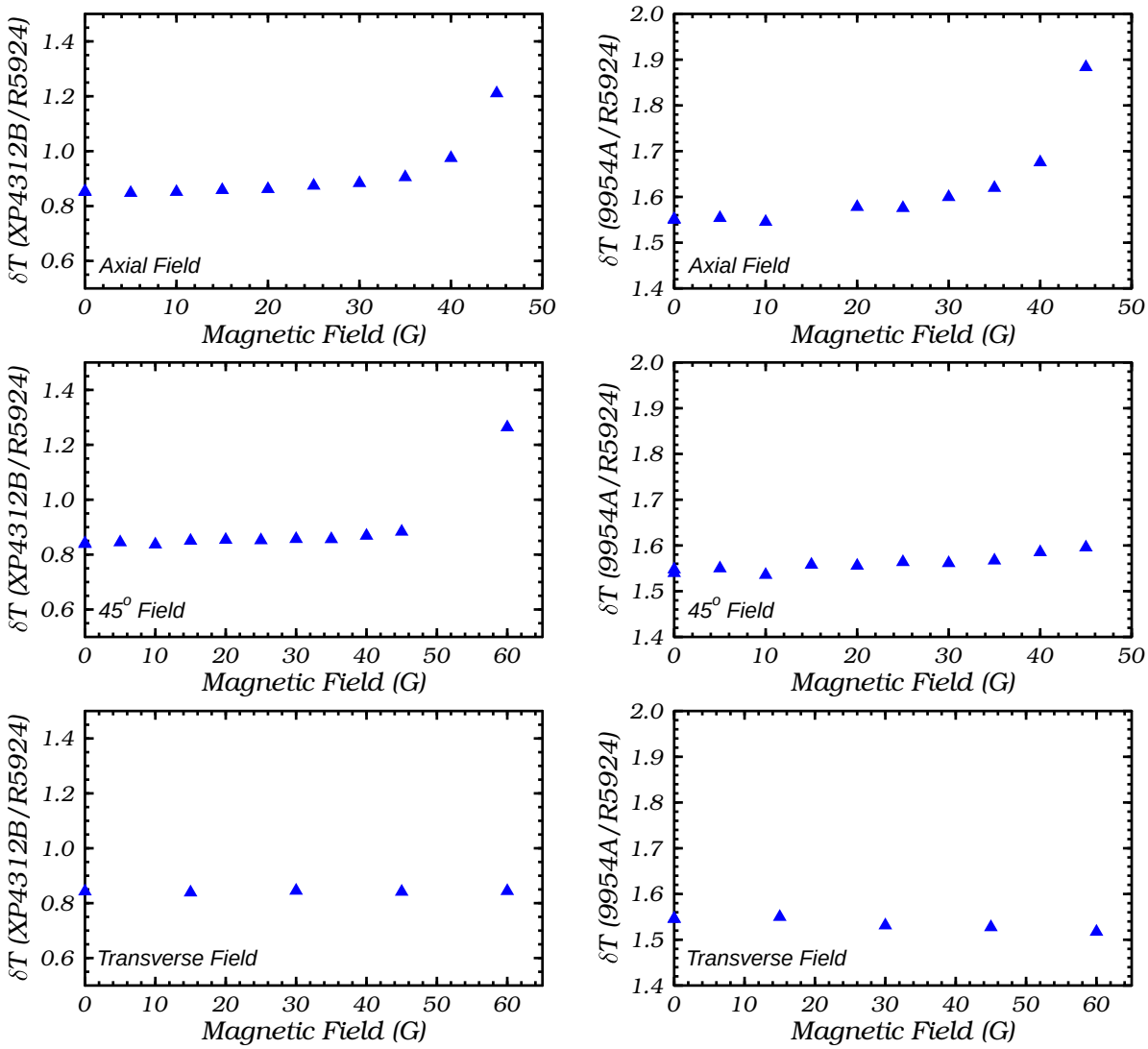

Figure 17: Main results of the PMT magnetic field dependence studies. The left column corresponds to the measurements with the 3-in XP4312B PMT and the right column corresponds to the measurements with the 2-in 9954A PMT. The top row shows the axial field measurements, the middle row shows the 45° measurements, and the bottom row shows the transverse field measurements. The timing resolution ratio of the test PMTs with respect to a field-immune R5924 PMT is shown plotted as a function of the magnetic field strength.

Appendix

	PMT coordinates (cm)			Solenoid field (G)			Torus field (G)			Total field (G)		
PMT	x	y	z	B_x	B_y	B_z	B_x	B_y	B_z	B_x	B_y	B_z
1	20.2	77.1	716.2	0.0	0.0	0.0	0.1	0.4	2.5	0.1	0.5	2.5
2	20.2	93.0	709.8	0.0	0.0	0.0	0.1	0.5	2.5	0.1	0.6	2.5
3	20.2	108.9	703.4	0.1	0.1	-0.1	0.1	0.7	2.5	0.2	0.7	2.4
4	20.2	124.7	697.0	0.2	0.2	-0.1	0.1	0.8	2.5	0.3	0.9	2.4
5	20.2	140.6	690.6	0.4	0.2	-0.3	0.1	0.9	2.5	0.5	1.1	2.2
6	22.4	155.2	684.2	0.6	0.4	-0.5	0.1	1.0	2.5	0.8	1.3	2.0
7	22.4	171.1	677.7	1.0	0.5	-0.7	0.1	1.1	2.5	1.2	1.6	1.7
8	22.4	187.0	671.3	1.6	0.6	-1.1	0.1	1.2	2.4	1.8	1.8	1.3
9	22.4	202.9	664.9	2.5	0.7	-1.6	0.1	1.3	2.4	2.6	2.0	0.8
10	22.5	218.7	658.5	3.4	0.8	-2.2	0.1	1.4	2.3	3.6	2.1	0.1
11	22.5	234.6	652.1	4.6	0.8	-2.8	0.1	1.4	2.2	4.7	2.2	-0.6
12	22.5	250.5	645.7	5.9	0.7	-3.5	0.1	1.5	2.2	6.0	2.3	-1.3
13	22.5	266.4	639.3	7.3	0.6	-4.1	0.1	1.6	2.1	7.5	2.2	-2.1
14	22.5	282.3	632.9	8.9	0.4	-4.8	0.1	1.6	2.0	9.0	2.0	-2.8
15	22.5	298.1	626.4	10.4	0.1	-5.5	0.1	1.7	1.9	10.6	1.8	-3.6
16	22.6	314.0	620.0	11.9	-0.4	-5.9	0.1	1.7	1.7	12.0	1.3	-4.2
17	22.6	329.9	613.6	13.2	-0.8	-6.3	0.2	2.2	1.8	13.3	1.3	-4.5
18	22.6	345.7	607.2	14.2	-1.3	-6.5	0.2	2.7	1.7	14.4	1.4	-4.8
19	22.6	361.6	600.8	15.0	-1.7	-6.6	0.2	3.2	1.5	15.2	1.4	-5.1
20	22.6	377.5	594.4	15.5	-2.1	-6.5	0.2	3.6	1.1	15.8	1.5	-5.4
21	22.6	393.4	588.0	15.8	-2.5	-6.2	0.2	3.9	0.5	16.0	1.4	-5.8
22	22.6	409.2	581.5	15.7	-2.7	-5.9	0.2	4.0	-0.2	15.9	1.2	-6.1
23	22.6	425.1	575.1	15.4	-2.9	-5.5	0.2	3.7	-1.0	15.6	0.8	-6.5

Table 2: Magnetic field values at the location of the FTOF panel-1a PMTs.

	PMT coordinates (cm)			Solenoid field (G)			Torus field (G)			Total field (G)		
PMT	x	y	z	B_x	B_y	B_z	B_x	B_y	B_z	B_x	B_y	B_z
1	18.0	48.5	712.1	0.0	0.0	0.0	0.1	0.3	2.6	0.1	0.3	2.6
2	18.0	54.8	709.6	0.0	0.0	0.0	0.1	0.3	2.6	0.1	0.3	2.6
3	18.0	61.3	707.0	0.0	0.0	0.0	0.1	0.4	2.6	0.1	0.4	2.6
4	18.0	67.6	704.4	0.0	0.0	0.0	0.1	0.4	2.6	0.1	0.4	2.6
5	18.0	74.1	701.8	0.0	0.0	0.0	0.1	0.5	2.6	0.1	0.5	2.6
6	18.0	80.4	699.2	0.0	0.0	0.0	0.1	0.5	2.7	0.1	0.5	2.6
7	18.0	86.9	696.6	0.0	0.0	0.0	0.1	0.6	2.7	0.1	0.6	2.6
8	18.0	93.3	694.1	0.1	0.1	0.0	0.1	0.6	2.7	0.2	0.7	2.6
9	18.0	99.7	691.4	0.1	0.1	-0.1	0.1	0.7	2.7	0.2	0.7	2.6
10	18.0	106.1	688.9	0.1	0.1	-0.1	0.1	0.7	2.7	0.2	0.8	2.6
11	18.0	112.5	686.3	0.2	0.1	-0.1	0.1	0.7	2.7	0.3	0.9	2.6
12	18.0	118.9	683.7	0.2	0.2	-0.2	0.1	0.8	2.7	0.4	1.0	2.5
13	18.0	125.4	681.1	0.3	0.2	-0.2	0.1	0.8	2.7	0.4	1.0	2.5
14	18.0	131.7	678.5	0.4	0.3	-0.3	0.1	0.9	2.7	0.5	1.1	2.4
15	18.0	138.2	675.9	0.6	0.3	-0.3	0.1	0.9	2.7	0.7	1.2	2.3
16	18.0	144.5	673.4	0.7	0.4	-0.4	0.1	1.0	2.7	0.8	1.3	2.2
17	18.0	151.0	670.7	0.9	0.4	-0.5	0.1	1.0	2.7	1.0	1.4	2.1
18	18.0	157.3	668.2	1.1	0.5	-0.6	0.1	1.1	2.6	1.2	1.5	2.0
19	18.0	163.8	665.6	1.4	0.5	-0.8	0.1	1.1	2.6	1.5	1.6	1.8
20	18.0	170.1	663.0	1.7	0.6	-0.9	0.1	1.2	2.6	1.8	1.7	1.7
21	18.0	176.6	660.4	2.0	0.6	-1.1	0.1	1.2	2.6	2.1	1.8	1.5
22	18.0	182.9	657.9	2.4	0.7	-1.3	0.1	1.3	2.6	2.5	1.9	1.3
23	18.0	189.4	655.2	2.8	0.7	-1.5	0.1	1.3	2.6	3.0	2.0	1.0
24	18.0	195.7	652.7	3.3	0.8	-1.7	0.1	1.3	2.5	3.4	2.1	0.8
25	18.0	202.2	650.1	3.8	0.8	-2.0	0.1	1.4	2.5	3.9	2.2	0.5
26	18.0	208.5	647.5	4.4	0.8	-2.2	0.1	1.4	2.5	4.5	2.2	0.3
27	18.0	215.0	644.9	5.0	0.8	-2.5	0.1	1.5	2.5	5.1	2.3	0.0
28	18.0	221.3	642.3	5.6	0.8	-2.8	0.1	1.5	2.4	5.8	2.3	-0.3
29	18.0	227.8	639.7	6.3	0.8	-3.1	0.1	1.5	2.4	6.4	2.4	-0.7
30	18.0	234.2	637.2	7.0	0.8	-3.3	0.1	1.6	2.4	7.2	2.4	-1.0
31	18.0	240.6	634.5	7.8	0.8	-3.6	0.1	1.6	2.3	7.9	2.4	-1.3
32	18.0	247.0	632.0	8.6	0.7	-3.9	0.1	1.6	2.3	8.7	2.3	-1.7

Table 3: Magnetic field values at the location of the small-angle FTOF panel-1b PMTs.

	PMT coordinates (cm)			Solenoid field (G)			Torus field (G)			Total field (G)		
PMT	x	y	z	B_x	B_y	B_z	B_x	B_y	B_z	B_x	B_y	B_z
33	18.0	253.4	629.4	9.4	0.6	-4.2	0.1	1.7	2.2	9.5	2.3	-2.0
34	18.0	259.8	626.8	10.2	0.5	-4.5	0.1	1.7	2.2	10.3	2.2	-2.4
35	18.0	266.3	624.2	11.0	0.4	-4.8	0.1	1.7	2.2	11.1	2.2	-2.7
36	18.0	272.6	621.6	11.8	0.3	-5.1	0.1	1.7	2.1	11.9	2.1	-3.0
37	18.0	279.1	619.0	12.7	0.2	-5.4	0.1	1.8	2.1	12.8	2.0	-3.3
38	18.0	285.4	616.5	13.5	0.1	-5.6	0.1	1.8	2.0	13.6	1.8	-3.6
39	18.0	291.9	613.8	14.3	-0.1	-5.9	0.1	1.8	2.0	14.4	1.7	-3.9
40	18.0	298.2	611.3	15.0	-0.3	-6.1	0.1	1.8	1.9	15.2	1.6	-4.2
41	18.0	304.7	608.7	15.8	-0.4	-6.3	0.1	1.8	1.9	15.9	1.4	-4.4
42	18.0	311.0	606.1	16.5	-0.6	-6.5	0.1	1.9	1.8	16.6	1.2	-4.7
43	18.0	317.5	603.5	17.2	-0.8	-6.6	0.1	1.9	1.8	17.3	1.1	-4.9
44	18.0	323.8	601.0	17.8	-1.0	-6.8	0.1	1.9	1.7	17.9	0.9	-5.0
45	18.0	330.3	598.3	18.4	-1.2	-6.9	0.1	1.9	1.7	18.5	0.7	-5.2
46	18.0	336.6	595.8	18.9	-1.4	-6.9	0.1	1.9	1.6	19.0	0.5	-5.3
47	18.0	343.1	593.2	19.4	-1.6	-7.0	0.1	1.9	1.6	19.5	0.3	-5.4
48	18.0	349.4	590.6	19.8	-1.8	-7.0	0.1	1.9	1.5	19.9	0.1	-5.5
49	18.0	355.9	588.0	20.1	-2.0	-7.0	0.1	1.9	1.5	20.2	0.0	-5.5
50	18.0	362.2	585.4	20.4	-2.1	-7.0	0.1	1.9	1.4	20.5	-0.2	-5.5
51	18.0	368.7	582.8	20.6	-2.3	-6.9	0.1	1.9	1.4	20.7	-0.4	-5.5
52	18.0	375.1	580.3	20.8	-2.5	-6.8	0.1	1.9	1.3	20.9	-0.6	-5.5
53	18.0	381.5	577.6	20.8	-2.6	-6.7	0.1	1.9	1.3	20.9	-0.7	-5.4
54	18.0	387.9	575.1	20.8	-2.8	-6.6	0.1	1.9	1.2	20.9	-0.8	-5.3
55	18.0	394.3	572.5	20.8	-2.9	-6.4	0.1	1.9	1.2	20.9	-1.0	-5.2
56	18.0	400.7	569.9	20.7	-3.0	-6.2	0.1	1.9	1.1	20.8	-1.1	-5.1
57	18.0	407.2	567.3	20.5	-3.1	-6.1	0.1	1.9	1.1	20.6	-1.2	-5.0
58	18.0	413.5	564.7	20.3	-3.1	-5.9	0.1	1.9	1.0	20.4	-1.3	-4.8
59	18.0	420.0	562.1	20.0	-3.2	-5.6	0.1	1.9	1.0	20.1	-1.3	-4.6
60	18.0	426.3	559.6	19.7	-3.2	-5.4	0.1	1.9	1.0	19.7	-1.4	-4.5
61	18.0	432.8	557.0	19.3	-3.3	-5.2	0.1	1.8	0.9	19.4	-1.4	-4.3
62	18.0	439.1	554.4	18.9	-3.3	-5.0	0.1	1.8	0.9	19.0	-1.4	-4.1

Table 4: Magnetic field values at the location of the large-angle FTOF panel-1b PMTs.

	PMT coordinates (cm)			Solenoid field (G)			Torus field (G)			Total field (G)		
PMT	x	y	z	B_x	B_y	B_z	B_x	B_y	B_z	B_x	B_y	B_z
1	10.1	455.8	541.5	27.9	-3.3	-3.6	0.0	1.8	0.8	27.9	-1.5	-2.8
2	10.2	469.6	522.5	21.6	-2.5	-2.7	0.0	1.9	0.6	21.7	-0.6	-2.1
3	10.3	483.2	503.6	23.0	-2.9	-2.6	0.0	1.9	0.5	23.0	-1.0	-2.1
4	10.2	497.0	484.7	23.6	-3.1	-2.4	0.0	1.9	0.4	23.6	-1.2	-2.0
5	10.2	510.7	465.8	23.4	-3.2	-2.1	0.0	1.9	0.3	23.5	-1.4	-1.8

Table 5: Magnetic field values at the location of the FTOF panel-2 PMTs.